Journal of Geodesy (2026) 100:88
https://doi.org/10.1007/s00190-026-02121-1

ORIGINAL ARTICLE

Effects of glacial loading in Svalbard on the VLBI scale realisation

Halfdan Pascal Kierulf[1] · Lisa Maria Kern[2] · Clinton Phillips Conrad[3] · Ann-Silje Kirkvik[1] · Hana Krásná[2] · Geir Moholdt[4] · Thomas Vikhamar Schuler[5]

Received: 5 February 2026 / Accepted: 16 September 2026
© The Author(s) 2026

Abstract

In the realisation of the International Terrestrial Reference System in 2000, and in the realisations since 2008, the scale of the International Terrestrial Reference Frame (ITRF) has been defined based on Very Long Baseline Interferometry (VLBI) and Satellite Laser Ranging (SLR) solutions, whereas ITRF2005 relied solely on VLBI. In the latest ITRF realisation, i.e. ITRF2020 with its first and second updates, VLBI sessions after September 2013 are excluded from the ITRF scale definition due to a detected drift in the VLBI solution with respect to the average scale trend computed from September 1997 until September 2013. Ny-Ålesund station in Svalbard, the northernmost fundamental geodetic station hosting all major techniques, plays a key role in ITRS realisation due to its location. Crustal motion measurements at Ny-Ålesund reveal nonlinear vertical motion, largely explained by elastic deformation caused by thinning glaciers. In the ITRF2020 updates (u2023 and u2024), a discontinuity in August 2016 was introduced for the VLBI station to account for the increasing uplift, reducing the detected scale drift relative to ITRF2020 by approximately 50%. In this study, we analyse the nonlinear vertical motion at Ny-Ålesund, compare it with predicted elastic loading signals arising from glacier thinning, and assess its impact on the VLBI scale estimates. Over the past 25 years, the land uplift rate increased from about 6 mm/year to 14 mm/year, indicating that the vertical displacement through time is not well described by a constant-rate model. The record also shows substantial interannual variability, of which the glacier loading model explains only about 50%. Including a nonlinear station motion model—based on Global Navigation Satellite System (GNSS) observations or loading predictions—for the VLBI station in Ny-Ålesund reduces the relative scale drift by 30–60%. Finally, we discuss alternative approaches to mitigate the negative effects of nonlinearity, such as modelling the elastic glacier signal or better integrating VLBI station motion with GNSS-derived displacement.

Keywords VLBI scale · Nonlinear land uplift · Glacier loading · ITRF

1 Introduction

A wide range of geodetic applications—from geo-referencing to precise satellite orbit determination—fundamentally rely on a stable, accurate, and globally consistent geodetic reference frame. The International Earth Rotation and Reference Systems Service (IERS, https://www.iers.org) coordinates three combination centres, each tasked with computing realisations of the International Terrestrial Reference System (ITRS). After a validation procedure, one realisation is defined to be the official International Terrestrial Reference Frame (ITRF) solution. The current official ITRF solution is the ITRF2020 realisation with its consecutive updates ITRF2020-u2023 and ITRF2020-u2024 (Altamimi et al. 2023), computed by the Institut National de l'Information Géographique et Forestière (IGN) in France.

The ITRF is defined by its origin, orientation, and scale at a reference epoch and its temporal derivatives. The accuracy and long-term stability requirements for the frame's origin and scale are one millimetre and one millimetre per decade, respectively, according to the goals of the Global Geodetic

✉ Halfdan Pascal Kierulf
halfdanpascal.kierulf@kartverket.no

1 Geodetic institute, Norwegian Mapping Authority, Hønefoss, Norway

2 Department of Geodesy and Geoinformation, TU Wien, Vienna, Austria

3 Centre for Planetary Habitability, University of Oslo, Oslo, Norway

4 Norwegian Polar Institute, Tromsø, Norway

5 Department of Geosciences, University of Oslo, Oslo, Norway

Published online: 30 September 2026

Observing System (GGOS; Plag and Pearlman 2009). This high-level requirement is essential for monitoring climate-change-related signals such as sea-level variation and crustal deformation.

In the realisation of the ITRS in 2000, and in the realisations since 2008 (Altamimi et al. 2011), the scale of the ITRF has been defined such that the scale and scale rate at the reference epoch are constrained to the average of the estimates from two space-geodetic techniques that provide independent scale information, namely Very Long Baseline Interferometry (VLBI) and Satellite Laser Ranging (SLR), whereas ITRF2005 relied solely on VLBI.

In the most recent realisation, ITRF2020, a drift of the VLBI-derived scale relative to the SLR scale was detected from around 2014 onward, with the underlying cause unidentified (Altamimi et al. 2023). To ensure a stable VLBI scale time series when defining the ITRF2020 scale, Altamimi et al. (2023) restricted the VLBI input to sessions with large and well-distributed networks prior to September 2013. This empirically chosen cut-off yielded the best agreement between the SLR- and VLBI-derived scales at epoch 2015.0 and no drift.

Following these findings, the VLBI community has put considerable effort into addressing the VLBI scale issue, including the establishment of a dedicated International VLBI Service for Geodesy and Astrometry (IVS) Working Group (WG9) to investigate the underlying causes of the drift in the relative scale parameter with respect to ITRF2020 observed after 2013.75.

Early investigations identified that the omission of several station events—such as repairs and readjustments in station motion models—as well as increasing uplift at Ny-Ålesund could contribute to the drift (Le Bail et al. 2023). Subsequent studies investigated the impact of additional discontinuities for stations affected by maintenance activities and equipment changes. Kern et al. (2024) found that their overall impact on the post−2013.75 scale is limited, while Le Bail et al. (2026) showed that such discontinuities can explain a small fraction of the observed relative scale drift. Nevertheless, both studies indicate that the effect of these discontinuities is considerably smaller than the contribution of the station motion mismodelling at Ny-Ålesund, where refining the model for the VLBI antenna produced a significant reduction in the relative scale drift. These findings are further supported by Ishigaki et al. (2026), who highlight the importance of NYALES20 for VLBI scale determination.

In the ITRF2020 updates, two discontinuities were introduced for the Ny-Ålesund VLBI antenna at epochs 2004.5 and 2016.6, consistent with those applied to the co-located Global Navigation Satellite System (GNSS) antennas NYAL and NYA1 already in ITRF2020. With these modifications—in particular the introduction of the 2016.6 break—the drift of the relative scale parameter between the VLBI solution and the reference frame was reduced by approximately 50%. The findings of Kern et al. (2025) further confirmed the importance of updating the station motion model at Ny-Ålesund for improving the VLBI scale stability.

These findings suggest that the post-2013 scale discrepancy between VLBI and SLR may not primarily be caused by VLBI-inherent mismodellings, but rather by inaccurate modelling of reference point displacement over time for particular stations. This is particularly relevant when the affected station is part of the datum-defining network, as the resulting discrepancies may be mapped into other estimated parameters, such as the relative scale factor between the VLBI solution and the reference frame. Especially in the case of VLBI, with its relatively sparse and varying station network, the effect is further pronounced for stations affected by strong nonlinear geophysical deformation and located in remote regions, such as the geodetic antennas located at Ny-Ålesund.

Arctic regions are experiencing some of the most rapid climatic changes on Earth, with temperatures increasing several times faster than the global average (Nordli et al. 2021). A direct consequence is the widespread retreat of Svalbard's glaciers (Morris et al. 2020; Schuler et al. 2020), which induces an elastic response of the solid Earth as the surface load decreases. This process has been extensively investigated in a series of studies focusing on Svalbard (e.g.Sato et al. 2006a, b; Kierulf et al. 2009a, b; Omang and Kierulf 2011; Mémin et al. 2011, 2012, 2014; Auriac et al. 2016; Rajner 2018; Kierulf et al. 2021, 2022; Schuler et al. 2025; Rajner 2025). Similar uplift patterns associated with glacier mass loss have been reported in Greenland (e.g. Khan et al. 2022) and Alaska (e.g. Naganawa et al. 2022). In both Greenland and Svalbard, uplift rates can reach several centimetres per year, and the magnitude of the deformation signal has increased in recent years; for example, Schuler et al. (2025) reported an uplift of 16.4 mm over a three-month summer period in 2024.

The aim of this study is to examine the influence of Ny-Ålesund as a datum station on the VLBI scale, with particular emphasis on displacement caused by the elastic response of the Earth to changing glacier load—an effect that is not accounted for in operational geodetic analysis.

The legacy 20-m VLBI telescope (NYALES20) at the Ny-Ålesund Geodetic Earth Observatory operated from 1994 until its decommissioning in August 2023 (see Fig. 1 for its location). In its final years, NYALES20 experienced technical challenges and decreased stability. Starting in 2020, NYALES20 operated alongside a newly installed 13-m twin telescope, located approximately 1.5 km away. This new system consists of two 13-m antennas, designated as north and south. The south antenna has participated in the legacy VLBI network since 2020, while the north antenna has contributed to the VLBI Global Observing System (VGOS) network since August 2022.

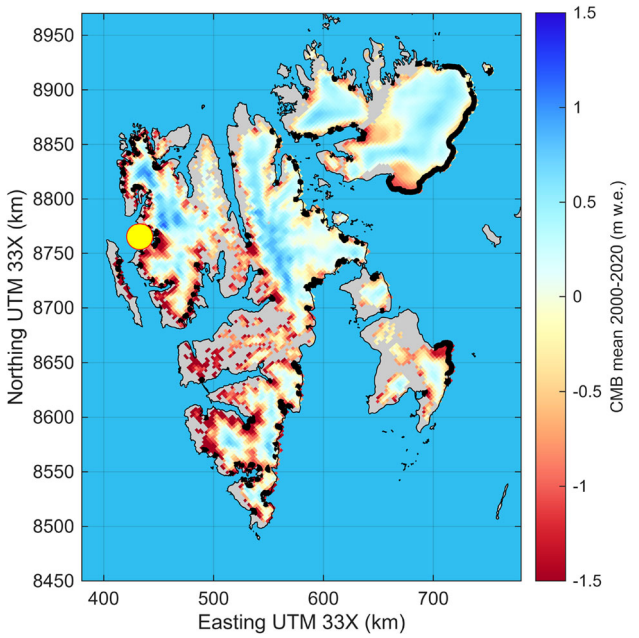

Fig. 1 Overview map of Svalbard illustrating the distribution of average Climatic Mass Balance (CMB) over 2000–2020. The yellow circle marks the location of the Ny-Ålesund fundamental geodetic station. The solid black line denotes marine glacier termini

The ITRF2020 realisation includes VLBI data until December 2020. In this study, we analyse data from 2000 to 2025, but unless otherwise stated, only observations up to the ITRF2020 cut-off date are used in the main comparisons.

In Sect. 2, we describe the geodetic data and methods used to estimate glacier mass change and to model the associated elastic deformation. Section 3 presents the kinematic behaviour of Ny-Ålesund and evaluates the impact of these motions on the terrestrial reference frame scale. In Sect. 4, other potential factors that could explain the uplift variations and the scale drift are considered and discussed.

2 Data and analysis

2.1 VLBI

The VLBI data, consisting of all suitable S/X legacy 24-hour VLBI sessions between 2000 and 2025 provided by the IVS, are analysed using the Vienna VLBI and Satellite Software (VieVS; Böhm et al. 2018). Within the VLBI analysis, the session-wise scale factor β relative to the a priori terrestrial reference frame, e.g. ITRF2020, can be determined when station positions are fixed to their a priori values. Earth Orientation Parameters (EOP) and radio source positions are estimated in a manner typical for operational VLBI analysis (see Table 1). The underlying assumption of this approach is that, if the a priori station coordinates and all applied models fully represented the observations, the estimated scale factor would be equal to unity. Consequently, any station motion that is not represented in the a priori model may be mapped, or aliased, into other estimated parameters. Thus, unmodelled nonlinear motion at a station such as NYALES20 may result in systematic effects in the estimated EOP and/or in the VLBI scale factor. However, owing to NYALES20's unique location, unmodelled vertical motion is expected to be particularly relevant to the estimated scale.

In VieVS, the partial derivative of the VLBI delay τ with respect to the scale factor β is given by

$$\frac{\partial \tau}{\partial \beta} = -\frac{\mathbf{k} \cdot \mathbf{b}}{c},$$

where $\mathbf{b}$ is the a priori baseline vector, $\mathbf{k}$ is the unit vector in the radio source direction, and c is the speed of light. In this context, β scales the baseline lengths to those provided by the a priori reference frame, and, therefore, reflects changes in the distances between the stations, not just in the radial direction. For more detailed information, see (MacMillan 2017) and Titov and Krásná (2018).

To assess the impact of elastic loading from glaciers at Svalbard on the global VLBI scale, we computed session-wise scale estimates relative to ITRF2020 and introduced additional, session- and time-dependent corrections to the station position of NYALES20 to account for these loading effects. Note that in the VLBI analysis, these corrections are applied in the same way as non-tidal loading displacement corrections, and all three local components (East, North, and Up) are taken into account.

In total, three scale time-series solutions were generated:

- SOL0 (reference solution): no additional station corrections applied.
- SOL1: station displacement model based on observed data from co-located GNSS antennas (see Sect. 2.2).
- SOL2: station displacement model based on the loading prediction from Loading Mass Balance (LMB) (see Sects. 2.3 and 2.4).

The station displacement model in SOL1 is the 60-day moving average of the detrended GNSS time series for NYA1. SOL2 is the detrended loading LMB time series for the same location. The models are detrended since the long-term rate for NYALES20 is already included in ITRF2020. This ensures as little consequence as possible for the solution, except for the effect of the nonlinear behaviour of the Ny-Ålesund site.

It should be noted that these solutions are analysed consistently and differ only in the additional displacement model applied to NYALES20. This allows the resulting scale time series to be directly compared and the impact of the applied

Table 1 VLBI analysis strategy

Option	Setting
General	
Sessions	IVS S/X legacy 24-h VLBI sessions
Time frame	2000 to 2025
Parameterisation	
Clocks	Piece-wise linear offsets (PWLO) with relative constraint of 43 ps (13 mm) after 1 h between offsets, one rate and quadratic term
Baseline clock offsets	Offsets at selected baselines Krasna et al. (2021)
Zenith wet delay	PWLO with relative constraint of 15 mm after 30 min between offsets
Tropospheric gradients	PWLO with relative constraint of 0.5 mm after 30 min between offsets
ERP	PWLO with relative constraint of 10 mas after 24 h
Celestial pole offsets	PWLO with relative constraint of 0.1 μas after 24 h
Station coordinates	Fixed to ITRF2020
Source coordinates	Estimated with no net rotation conditions on ICRF3 defining sources
Scale factor	Estimated

mas = milliarcseconds; μas = microarcseconds

geophysical loading corrections on the VLBI scale factor to be assessed. Since no subset of datum-defining stations has been defined, all stations contribute to the scale determination. Consequently, individual sessions with weak network geometry, or particular stations or baselines with a limited number of observations or poor long-term stability, may affect the estimated scale factor. These effects are largely common to all three solutions and therefore have a limited impact on the relative comparison between them. However, to reduce the influence of unstable and unreliable estimates, outliers are removed from the scale time series and moving averages are provided in the following to emphasise the long-term behaviour.

2.2 GNSS

The GNSS data are analysed using the GAMIT/GLOBK (Herring et al. 2018) software package (v10.71) and following the IGS-repro3 analysis strategy guidelines http://acc.igs.org/repro3/repro3.html. We have analysed data on a daily basis from a network of GNSS stations in the Arctic. The network is combined with a global network of stations from International GNSS Service (IGS). This ensures a good connection to the ITRF. The GNSS stations NYA1 and NYAL have been operational since 1997 and 1993, respectively, and are located around 100 metres from the NYALES20 VLBI antennae. Coordinate time series for these two stations are extracted from the GNSS solution.

2.3 Glacier mass balance

Glacier mass changes occur mostly across the surface through accumulation of snow or runoff of meltwater, as well as at marine-terminating ice fronts, where subaqueous melting and calving of icebergs considerably contribute to mass reduction. The budget of climatically driven snowfall and melting is termed the Climatic Mass Balance (CMB), whereas the loss term at the fronts of glaciers that reach into the ocean is known as Frontal Ablation (FA); together, these components make up the Total Mass Balance (TMB). However, since submarine glacier retreat is replaced by water—and the opposite in the case of advance—terminus fluctuations have minimal impact on loading, so we ignore this part of FA and only consider Solid Ice Discharge (SID), which represents a transfer of mass from the glacier interior to the ocean at the marine-terminating fronts. Mass loss due to changes in glacial flow is accounted for in the FA term (see Sect. 2.4 for details).

To estimate the CMB, we have used the dataset by Schmidt (2022), based on simulations of the surface energy balance. The CryoGrid community model (Westermann et al. 2023) has been forced by the Copernicus Arctic Regional ReAnalysis (CARRA)(Schyberg et al. 2020) reanalysis (1991–2025) and is updated in near-real time using operational AROME-ARCTIC forecasts (Bengtsson et al. 2017). For more details, see (Schmidt et al. 2023). The gridded CMB product has a spatial resolution of 2.5 km and a daily temporal resolution, and covers the whole of Svalbard (see Fig. 1). For the ~200 glaciers of Svalbard that reach into the ocean, SID has been estimated by a combination of remotely sensed glacier speed and ice thickness estimates at the evolving marine-terminating fronts, as described by Foss et al. (2024). The SID dataset can be found in Moholdt et al. (2021). This dataset starts in the end of summer 2012, and SID data prior to this is extrapolated based on the first year of the dataset (2012-2013). We define the LMB as the sum of CMB and SID,

i.e. LMB is the part of TMB that is relevant for the loading estimation.

2.4 Loading

Earth's crust responds to different loadings as an elastic body (Petrov and Boy 2004). Tidal loadings, such as ocean tide loading and the ocean pole tide, are included in GNSS and VLBI analyses contributing to the ITRF combination, whereas non-tidal loadings from Atmosphere (ATM), Non-Tidal Ocean (NTO), and Land Water Storage (LWS) are not. Loading from ATM and NTO do not have a significant impact on the rates over longer timescales, while LWS can exhibit changes over yearly timescales. Mielke et al. (2025) found a significant nonlinear trend in the GNSS time series and explained it by changes in LWS due to multiple droughts. Yearly glacier changes accumulate over time and can produce a significantly varying, nonlinear uplift signal in glaciated areas (see, e.g. Khan et al. 2022; Kierulf et al. 2022).

The ice-loading predictions were calculated using convolution with Green's functions (Farrell 1972), which describe the Earth's response to surface mass changes. The Green's functions depend on the distance to the actual load change. The ground motion in response to CMB is obtained by convolving the mass changes at each grid point in the model. We assume that the mass change by SID takes place where the ice flows from land into the ocean (Fig. 1) while in nature this mass is partly advected from up glacier, but this is difficult to determine. We have used the distance from NYA1 to the respective glacier front to obtain the weight used in the convolution.

2.5 Time-series analysis

Geodetic time series are often affected by correlated noise (Williams et al. 2004; Bos et al. 2008; Li et al. 2024). Neglecting this correlation typically leads to underestimated uncertainty estimates. The time-series analysis software Hector (Bos et al. 2008) supports modelling various types of correlated noise. VLBI observations are campaign-based, with irregular intervals between sessions and varying network geometry and quality. Li et al. (2024) tested the use of Hector on irregularly sampled VLBI time series. They concluded that, with more than 300 data points in the time series, reliable noise estimation results can be obtained. The VLBI scale time series used in this study contains more than 2000 data points over a 25-year period. Hector does not take formal errors into account in the analysis; the effect of this is discussed in Sect. 3.3. All time series in this study are analysed using Hector with a noise model comprising white noise and a power-law component. We have also used the Akaike Information Criteria (AIC) and Bayesian Information Criteria (BIC) values reported by Hector to discriminate between different models in the time-series analysis.

3 Results

3.1 Uplift

In Fig. 2, the vertical coordinate time series for the NYA1 GNSS antenna is shown. The site exhibits a long-term uplift of 9.2 $\pm$ 0.3 mm/year averaged over the last 25 years, with clear seasonal and interannual signals. The average annual amplitude is 4.5 $\pm$ 0.5 mm, although the seasonal signal varies significantly from year to year. For example, note the pronounced seasonal uplift anomalies in 2020 and 2024.

Figure 3 illustrates the average uplift rates for moving windows of 5-year periods. A similar pattern is observed for the two GNSS stations, NYAL and NYA1, as well as the VLBI station NYALES20. The land uplift rate was below 6 mm/year in the late 1990s and is now approaching 14 mm/year, depending on the selected time period and time-series length. The uncertainties for different 5-year time intervals are between 1.1 and 1.5 mm/year for the GNSS time series.

The uplift rates based on GNSS include several processes, such as tectonics, GIA, and various elastic loadings. The predicted uplift rates from LMB alone are therefore smaller. The evolution of the predicted loading rates from LMB is shown in Fig. 3. The predicted uplift-rate changes are about 50% lower than those measured with GNSS. The tectonic and GIA signals are generally considered constant and are therefore not expected to explain the observed variations in the rate change (see the discussion in Sect. 4.3). Kierulf et al. (2022) estimated the constant non-LMB uplift to be approximately 6.8 mm/year. We will discuss these discrepancies in Sect. 4.

In ITRF2020 and subsequent updates, a rate change was introduced for the GNSS stations in Ny-Ålesund at 2016.6. For the VLBI station NYALES20 a rate change at 2016.6 was first introduced with the ITRF2020 updates. Table 2 summarises the rates before this date and the magnitude of the rate change, including values from our GNSS solution. Notably, the uplift rate for NYA1 has continued to increase after 2016.6 as more data were incorporated in the ITRF2020 updates.

To ensure the stability of the geodetic observatory in Ny-Ålesund, repeated local ties have been measured using total stations, levelling, and GNSS vectors (Tangen et al. 2024). The first local-tie campaign was conducted in 2002, followed by annual campaigns since 2018. No significant instability of the control points for the main geodetic instruments has been detected. In particular, the vector between the VLBI point NYALES20 and the GNSS points NYAL and NYA1 has remained stable within the uncertainty level. We there-

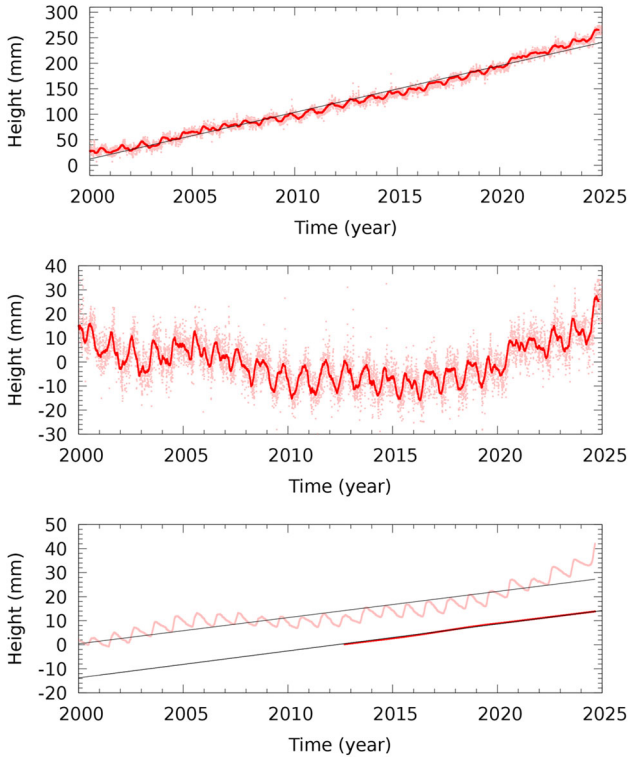

Fig. 2 Uplift in Ny-Ålesund. The upper panel shows the GNSS time series from NYA1; the middle panel shows the corresponding detrended time series. Pink dots are the daily coordinates, and red curves are the 60-day moving average. The lower panel shows the predicted uplift from the CMB model (pink) and the SID model (red). The SID model is extrapolated before 2012

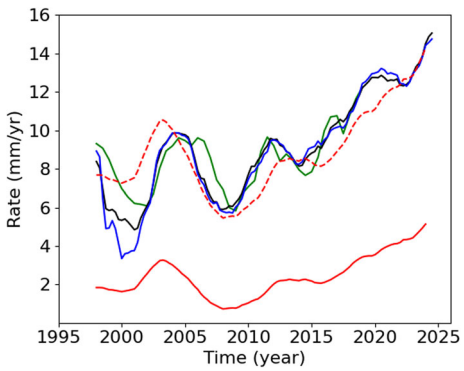

Fig. 3 Interannual uplift variations in Ny-Ålesund. Rates are based on a 5-year moving window for the GNSS stations NYAL (blue) and NYA1 (black) and the VLBI station NYALES20 (green). The red curve shows the glacial elastic loading prediction from LMB; the dashed red curves show the same signal, but multiplied by two and shifted upwards by 4 mm/year for comparison. The curves are plotted on the midpoint of the 5-years moving window. NYA1 has been operational since June 1997, and we use data until December 2025; hence, values before 2000 for NYA1 and after 2022.5 for all curves are based on less than 5 years of data. Both NYA1 and NYAL underwent equipment changes in the late 1990, which may explain the irregularities at the beginning of the curves

Table 2 Rate and rate change in 2016.6

	Uplift 2000.0–2016.6	Uplift change post 2016.6
GNSS: NYA1*	7.8 ± 0.4	4.7 ± 1.4
GNSS: NYAL*	7.7 ± 0.4	4.8 ± 1.2
GNSS: NYA1**	7.8 ± 0.3	5.0 ± 0.7
GNSS: NYAL**	7.7 ± 0.4	5.2 ± 0.7
Results from ITRF solutions		
ITRF2014: NYA1	7.7	–
ITRF2014: NYALES20	7.7	–
ITRF2020: NYA1	7.6	2.6
ITRF2020-u2023: NYA1	7.5	4.0
ITRF2020-u2024: NYA1	7.5	4.2
ITRF2020: NYALES20	7.9	–
ITRF2020-u2023: NYALES20	7.5	3.6
ITRF2020-u2024: NYALES20	7.5	3.7

All numbers are in mm/year. (∗) includes data up to 2021.0; (∗∗) includes data up to 2025.0. Note the tendency towards a larger rate change when including data beyond 2021. The ITRF results are taken from the ITRF solutions and transformed from Cartesian coordinates to vertical uplift

fore conclude that the discrepancies in observed uplift in this study are mainly caused by the influence of nonlinear ground motion across different time intervals.

3.2 Scale

Figure 4 (upper panel) shows the session-wise VLBI scale estimates relative to ITRF2020 (the SOL0 solution), the 90-day moving average, and the step-wise linear function of the scale results. We observe a clear change in the relative scale rate at the beginning of the 2010s, and the step-wise linear function includes a rate shift at 2013.75, but no offset.

Table 3 presents the results of the time-series analysis of the different VLBI scale estimates, assuming rate shifts at 2013.75 or 2016.6. We observe a clear reduction in the rate shift for the modified solutions SOL1 and SOL2. The rate shifts were reduced by approximately 60% and 30%, respectively. The AIC and BIC values reported by Hector prefer the solution with a scale-rate change in 2013 for all the solutions.

Although the relative scale rates after 2013.75 (and 2016.6) are clearly reduced for both SOL1 and SOL2, they still deviate significantly from zero. The remaining discrepancies will be discussed further in Sect. 4. The scale rates before 2013.75 (and 2016.6) are not significantly different from zero, except for the SOL1 solution. The apparent trend

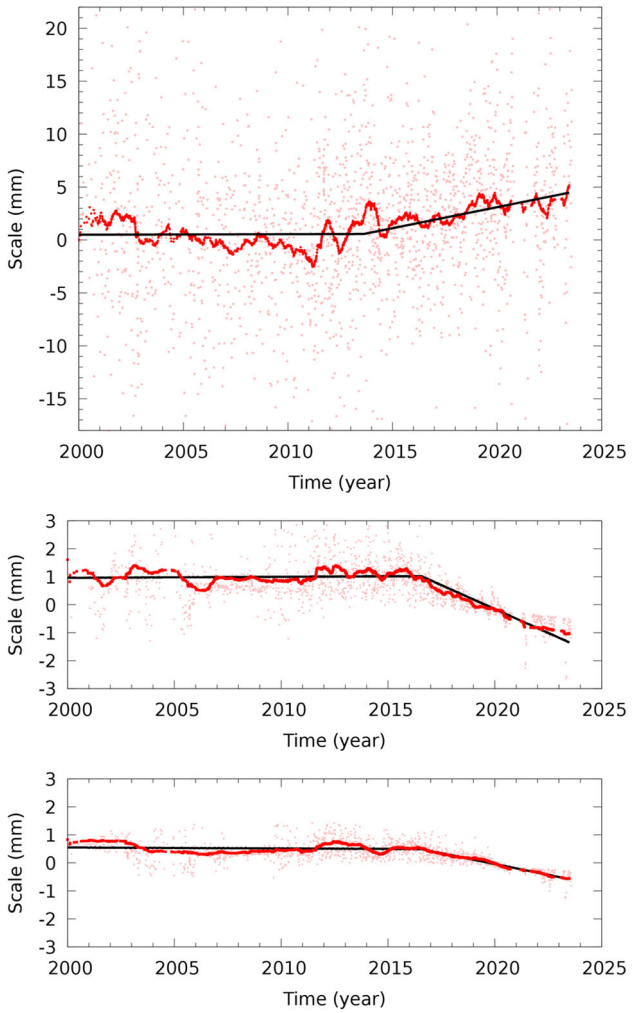

Fig. 4 VLBI scale variations. The values are converted to mm. The red dots are session-wise scale values. Red curves are 60-day moving averages. The upper panel shows the scale of the SOL0 solution, i.e. relative to the ITRF2020. The middle and lower panels show the scale differences for the SOL1 and SOL2 solutions, respectively, relative to the SOL0 solution

of 0.15 ± 0.12 mm/year in SOL1 before 2013.75 arises from an apparent negative uplift trend in Ny-Ålesund. Due to increased uplift towards the end of the time series, the detrended time series appears negative in the early part. Consequently, the scale rate relative to this modified trend in Ny-Ålesund (SOL1) appears to be positive.

In Fig. 4 (middle panel), the differences in scale estimates between the modified solution SOL1 and the reference solution are shown. In the lower panel, the corresponding differences for the modified solution SOL2 are shown. The effect of modifying the station displacement model for NYALES20 is clearly evident. The estimated values are included in Table 4. The AIC and BIC values reported by Hector prefer the solution with a scale-rate change in 2016 for both difference series.

3.3 Noise and noise characteristics

The uncertainties reported in Tables 3 and 4 were estimated using Hector, assuming a noise model comprising white noise and a power-law component (Sect. 2.5). The estimated power-law indices for the scale time series are −0.89, −0.99, and −1.00 for the SOL0, SOL1, and SOL2 solutions, respectively. The fraction of power-law noise is less than 2% in all three solutions. Although this fraction is small, including power-law noise increases the estimated rate uncertainty by approximately a factor of two compared to estimates using only white noise. For the difference time series SOL1–SOL0 and SOL2–SOL0, the power-law indices are −1.3, and the fractions of power-law noise are 5% and 2.5%, respectively. However, the total noise level is much lower for the difference time series, and consequently, the uncertainties are smaller, as shown in Table 4.

The formal errors in VLBI scale time series vary and depend strongly on network geometry. Hector does not take these formal errors into account, which may affect the estimated rates and associated uncertainties. To assess the robustness and accuracy of our results, we modified the time series by applying thresholds to the formal uncertainties of the VLBI scale data included in the analysis. By applying increasingly strict uncertainty thresholds to the included VLBI sessions, we observe no significant change in the estimated trends. However, the uncertainties decrease slightly for time series composed of fewer, higher-quality sessions. The noise in these time series exhibits lower variability, and the power-law index approaches zero, indicating behaviour closer to white noise. This explains the reduced uncertainties despite the smaller number of observations.

4 Discussion

Our uplift analysis of five-year time series derived from VLBI and GNSS observations in Ny-Ålesund shows variability of approximately 8 mm/year (ranging from ∼6 to ∼14 mm/year). However, the elastic loading associated with the LMB model accounts for only a fraction of this signal. In the late 1990 s, both NYAL and NYA1 experienced equipment upgrades that may have introduced biases in the estimated rates. When excluding time spans affected by these equipment changes (i.e. considering data from approximately 2002 onwards; see Fig. 3), the LMB model explains roughly half of the observed variability.

If nonlinear behaviour, such as vertical land motion caused by LMB, is not property accounted for in a data defining network, the resulting displacements may propagate into other estimated parameters, such as the relative scale factor between the VLBI solution and the reference frame.

Table 3 Scale rates

	Before 2013.75	After 2013.75	Scale-rate change	Reduction
SOL0	-0.01 ± 0.10	0.53 ± 0.18	0.54	–
SOL1	0.15 ± 0.12	0.34 ± 0.21	0.19	64%
SOL2	0.06 ± 0.11	0.43 ± 0.20	0.37	31%
	Before 2016.6	After 2016.6	Scale-rate change	Reduction
SOL0	0.05 ± 0.09	0.83 ± 0.35	0.78	–
SOL1	0.16 ± 0.10	0.47 ± 0.37	0.31	60%
SOL2	0.10 ± 0.10	0.64 ± 0.38	0.55	29%

The values are converted to mm/year. The reduction is relative to the ITRF2020 reference solution (SOL0)

Table 4 Relative scale rates

	Before 2013.75	After 2013.75	Scale-rate change
SOL1–SOL0	0.15 ± 0.05	-0.17 ± 0.08	-0.32
SOL2–SOL0	0.07 ± 0.02	-0.08 ± 0.04	-0.14
	Before 2016.6	After 2016.6	Scale-rate change
SOL1–SOL0	0.11 ± 0.04	-0.28 ± 0.13	-0.38
SOL2–SOL0	0.05 ± 0.02	-0.15 ± 0.05	-0.20

The values are converted to mm/year. The scale rates are for the modified solutions (SOL1 and SOL2) relative to the reference solution (SOL0)

Applying a station displacement model for NYALES20 reduces the detected drift in the VLBI scale with respect to ITRF2020. By linking the motion of NYALES20 to the nonlinear movements of the GNSS station NYA1, we achieve a reduction in scale drift of approximately 60%. The effect of using a station displacement model based on GNSS is similar to introducing a break in the VLBI time series, as reported in Kern et al. (2025).

As shown in Fig. 4, Tables 3, and 4, the effect of modifying the station displacement model mainly appears from 2016. However, the reduction in scale rate with respect to ITRF2020 is evident when estimating scale-rate changes for both 2013 and 2016.

When using a station displacement model based on the glacial loading model, the effect is approximately 30% , i.e. about half of that obtained with a GNSS-based model. This is consistent with the finding that the elastic loading model explains only about 50% of the observed uplift variability. The possible causes of these discrepancies are discussed in detail in Sects. 4.1 through 4.3. Our results account for up to approximately 60% of the relative scale drift. Possible causes of the remaining discrepancy are discussed in Sect. 4.4.

4.1 Svalbard glacier mass balance and loading

CMB simulations have been carefully evaluated by Schmidt et al. (2023), comparing model results with in situ measurements of glacier mass balance as well as mass change estimates derived from satellite measurements of surface-elevation changes. While in situ measurements are useful to evaluate the spatial pattern and temporal variation of CMB, the altimetry-based techniques can quantify the volume change with high accuracy over multi-year timescales, which is then converted to mass change by assumptions of material density (Huss 2013). Schmidt et al. (2023) found generally good agreement with in-situ and satellite data, as well as with other published CMB simulations (see Fig. 12 in Schmidt et al. (2023)).

For a stable glacier, CMB is balanced by ice submergence/emergence and ice discharge at the front. However, Svalbard glaciers are out of equilibrium with the climate, and most of the loading change (thinning) occurs at the lower parts of the glaciers where CMB is most negative. We therefore use CMB directly as a proxy for local loading change. The SID results from dynamic thinning occurring throughout the glacier systems, and identifying the precise location of associated loading changes is therefore possible only if spatial data on ice thickness changes are available. In the absence of such data, we assume that SID loading changes occur at the glacier fronts. Given that the major glaciers surrounding Ny-Ålesund have flow directions approximately towards the geodetic stations, the effective distances to the assumed loading points might be at the lower end, potentially causing a slight overestimation of the predicted uplift signal from the SID.

We have tested the sensitivity of assuming that the SID loading change occurs at the calving front, rather than the true but unknown location of the loading change, by increasing the distance to the SID. The estimated uplift from the SID varies between 0.9 mm/year and 1.3 mm/year. Increasing the distance to the loading change for the glaciers surrounding Ny-Ålesund by 10 kilometres reduces the predicted signal by 0.1 mm/year.

4.2 Loading from Greenland and other glacier regions

The Greenland ice sheet is about 50 times larger than the glaciers on Svalbard, but due to its slower changes and larger distance from Svalbard, the associated uplift signal is relatively small. We computed the elastic loading signal from Greenland using glacial data described in Khan et al. (2022) and the CMB described in Mankoff et al. (2021). The resulting average uplift signal at Ny-Ålesund is approximately 0.5 mm/year, reaching nearly 1.0 mm/year in 2012 and 2019—years with particularly negative mass balance in Greenland.

The contributions from other Arctic glaciers are minimal. Using the altimetry-based dataset of ice thickness change from Smith et al. (2024), we computed the associated uplift signals from the Russian Arctic, Canada, and Iceland. For the period 2019–2024, these signals were 3.3%, 1.7%, and 0.3%, (respectively), of the signal from Svalbard glaciers.

4.3 Visco-elastic loading

The results suggest that rates of uplift observed at Ny-Ålesund are approximately double those expected from purely glacial elastic deformation of the Earth (Fig. 3). This is surprising because the visco-elastic response to glacial unloading is generally considered to be dominated by elastic deformation on the annual to decadal timescales considered here. Elastic uplift rates may be sensitive to regional heterogeneity in the elastic properties of shallow crustal structure, but only for locations that are less than about 1 km from unloading areas (Durkin et al. 2019). For Ny-Ålesund, the closest ice is 2.5 km away, and thus the modelled elastic response should be relatively robust (Mitrovica et al. 2011). Therefore, an alternative explanation is needed to explain unusually rapid uplift at Ny-Ålesund. One possibility could be an accelerated viscous response to recent melting. We note that the viscous response to deglaciation is sensitive to upper mantle viscosity and may be important on timescales as short as years to decades where the viscosity of the uppermost mantle is reduced to $\sim 10^{18}$ Pa s (e.g. Nield et al. 2014; Khan et al. 2016; Weerdesteijn et al. 2022). For example, recent uplift in southwest Greenland has been attributed to a rapid viscous response to extensive recent deglaciation occurring above mantle rocks that have been weakened by heat from the Iceland Plume (Weerdesteijn and Conrad 2024).

For western Svalbard, magnetotelluric constraints suggest the presence of a warm layer containing partial melt beneath the lithosphere, with viscosities as low as $\sim 10^{18}$ Pa s (Selway et al. 2020). This weakened upper mantle is consistent with a warm upper mantle associated with the nearby western Gakkel Ridge (Minakov 2018), as well as late Cenozoic intraplate volcanism across northern Svalbard and offshore (Meza-Cala et al. 2024). Similarly low asthenospheric viscosity, in the range of 10^{18} to 10^{19} Pa s, has been proposed previously for Ny-Ålesund to explain uplift rates following Little Ice Age deglaciation (Mémin et al. 2014), and may be relevant to describe land emergence out of the broader Barents Sea (Kaufmann and Wolf 1996; Steffen and Kaufmann 2005). If mantle rheology is nonlinear and timescale-dependent (e.g. Lau et al. 2021), then Svalbard's recent and rapid deglaciation may serve to reduce effective viscosities even further, as has been suggested for Greenland (e.g. Paxman et al. 2023). All of these factors may weaken the upper mantle beneath western Svalbard, and would facilitate a rapid viscous response to recent deglaciation that could drive faster-than-expected uplift at Ny-Ålesund. Study of this hypothesised viscous component of uplift represents an avenue for future research.

4.4 Other effects affecting the VLBI scale

The impact of the NYALES20 displacement modelling, derived from the two evaluated nonlinear motion models, on the scale estimates from VLBI sessions is evident from 2016 onwards (Fig. 4, middle and lower panels). However, Altamimi et al. (2023) empirically localised the start of the VLBI scale drift at epoch 2013.75, which yielded the best scale agreement between SLR and VLBI from 1997.75 to 2013.75. This suggests that additional factors may influence the TRF scale determination, highlighting the importance of careful review of geodetic results.

The IVS community has recently focused on a number of issues in the delay modelling, which have an impact on the TRF scale determination from VLBI observations. Nothnagel et al. (2026) discovered inconsistencies, and in some cases, erroneous values for ionospheric calibrations of the S/X VLBI sessions, stored in the databases distributed through IVS Data Centres. They show an effect on the VLBI scale estimates on average of about −0.6 mm after a sudden jump in 2022, which in extreme cases reaches up to −2 mm. Another network-dependent bias in the VLBI scale offset with respect to ITRF2020 after 2015 has been attributed to the Sejong telescope, actively observing since December 2014, based on its new value for the telescope axis offset determined by precision surveying in 2025 (Yi and Hong 2025).

Based on these findings, the IVS has recently initiated a full reprocessing of the VLBI geodetic data for the next ITRF realisation.

5 Conclusions

In the consecutive updates of ITRF2020, a discontinuity was introduced for NYALES20 in 2016 to account for nonlinear motion, reducing the VLBI scale drift with respect to the

SLR solution by approximately 50%. However, unnecessary or unexplained discontinuities are undesirable in geodetic time series used for reference frame realisation. We have shown that introducing alternative station motion models for NYALES20 can further reduce the scale drift without adding new discontinuities. The first model, derived from the co-located GNSS station NYA1, reduced the scale drift by 64%.

While the GNSS-derived model yields the largest reduction in the drift of the relative scale factor between VLBI solutions and the ITRF2020, its use inherently introduces a dependence of the VLBI solution on GNSS-derived station motion. This conflicts with the principle of technique independence in ITRF realisations. It also causes problems for single-technique operational analyses, where such GNSS-derived models are not available; this favours displacement models based on geophysical models independent of the ITRF.

Initiatives to combine space-geodetic techniques at the observation level—such as the integrated GPS–VLBI processing demonstrated by Wang et al. (2025)—offer a more rigorous framework for a multi-technique combination that leverages the strengths of individual techniques. The GENESIS mission (European Space Agency 2024) will provide new opportunities to study and control cross-dependencies between space-geodetic techniques through a physically realised space tie, helping to isolate technique-specific contributions to the terrestrial reference frame. These developments highlight the need for physically based station motion models when aiming to improve the consistency and stability of future reference frame realisations.

The second model, based on elastic modelling of the Earth's response to recent deglaciation in Svalbard, achieved a 31% reduction. The magnitude of vertical uplift predicted by this loading model is approximately half of that observed in the GNSS time series, explaining the smaller improvement. Potential explanations for this discrepancy include uncertainties in the Svalbard mass balance (Sect. 4.1), vertical loading from Greenland (Sect. 4.2), and—perhaps most importantly—a low upper mantle viscosity beneath Ny-Ålesund that could allow a rapid viscous response not captured by the elastic modelling (Sect. 4.3). Signals from other loading sources, e.g. changes in non-frozen water or tectonic processes, cannot be excluded. Future work addressing these factors may help to develop physically based predictive displacement models for Arctic stations.

NYALES20, with its unique northern location, long time series, and high temporal resolution, makes it essential for the quality and stability of datum parameters such as scale. At the same time, scale is highly sensitive to mismodelling of station motion, which again emphasises the need for proper handling of station motion.

As the accuracy of geodetic reference frames such as the ITRF continues to improve, user requirements for precision increase correspondingly. This underscores the need for improved quality and a deeper understanding of the kinematic behaviour of the stations defining the reference frame. Moreover, the accelerating impacts of climate change on geodetic networks—especially in the Arctic—highlight the necessity of adapting station motion models and implementing them effectively in future ITRF realisations.

Acknowledgements The authors acknowledge the IVS and IGS and all their components for providing VLBI and GNSS data. We thank the editors Hansjörg Kutterer and Susanne Glaser and three anonymous reviewers for their constructive comments that helped improve the manuscript.

Author Contributions HPK conceived the manuscript idea, designed the research, performed the GNSS and time-series analyses, and interpreted the results. LK carried out the VLBI analysis. All authors contributed to the investigation and to the writing of the manuscript.

Funding This work was supported by the Research Council of Norway (project 332523) through CPC.

Data Availability VLBI data used in this study are available from the Crustal Dynamics Data Information System (CDDIS) archive at https://cddis.nasa.gov/archive/vlbi. GNSS data can be downloaded from the IGS data centres https://igs.org/data-access/#global-dcs. The CMB dataset is available in Schmidt (2022), and the SID dataset in Moholdt et al. (2021).

Open Access This article is licensed under a Creative Commons Attribution 4.0 International License, which permits use, sharing, adaptation, distribution and reproduction in any medium or format, as long as you give appropriate credit to the original author(s) and the source, provide a link to the Creative Commons licence, and indicate if changes were made. The images or other third party material in this article are included in the article's Creative Commons licence, unless indicated otherwise in a credit line to the material. If material is not included in the article's Creative Commons licence and your intended use is not permitted by statutory regulation or exceeds the permitted use, you will need to obtain permission directly from the copyright holder. To view a copy of this licence, visit http://creativecommons.org/licenses/by/4.0/.

References

Altamimi Z, Collilieux X, Métivier L (2011) ITRF2008: an improved solution of the international terrestrial reference frame. J Geodesy 85:457–473. https://doi.org/10.1007/s00190-011-0444-4

Altamimi Z, Rebischung P, Collilieux X et al (2023) ITRF2020: an augmented reference frame refining the modeling of nonlinear station motions. J Geodesy 97(5):47. https://doi.org/10.1007/s00190-023-01738-w

Auriac A, Whitehouse P, Bentley M et al (2016) Glacial isostatic adjustment associated with the Barents Sea ice sheet: a modelling inter-comparison. Quat Sci Rev 147:122–135. https://doi.org/10.1016/j.quascirev.2016.02.011

Bengtsson L, Andrae U, Aspelien T et al (2017) The harmonie-arome model configuration in the aladin-hirlam nwp system. Mon Weather Rev 145:1919–1935. https://doi.org/10.1175/MWR-D-16-0417.1

Böhm J, Böhm S, Boisits J, et al (2018) Vienna vlbi and satellite software (vievs) for geodesy and astrometry. Publ Astron Soci Pacific 130(986). https://doi.org/10.1088/1538-3873/aaa22b

Bos M, Fernandes R, Williams S et al (2008) Fast error analysis of continuous GPS observations. J Geodesy 82:157–166. https://doi.org/10.1007/s00190-007-0165-x

Durkin W, Kachuck S, Pritchard M (2019) The importance of the inelastic and elastic structures of the crust in constraining glacial density, mass change, and isostatic adjustment from geodetic observations in southeast alaska. J Geophys Res Solid Earth 124(1):1106–1119. https://doi.org/10.1029/2018JB016399

European Space Agency (2024) Genesis: new combined processing. Presentation at the 9th International Colloquium on Scientific and Fundamental Aspects of GNSS, https://dgnl7.esoc.esa.int/attachments/125054211/1/Presentation_-_GENESIS_New_Combined_Processing_-_final.pdf, ESA/ESOC Navigation Support Office

Farrell WE (1972) Deformation of the Earth by surface loads. Rev Geophys Space Phys 10(3):761–797. https://doi.org/10.1029/RG010i003p00761

Foss Ø, Maton J, Moholdt G et al (2024) Ocean warming drives immediate mass loss from calving glaciers in the high Arctic. Nat Commun 15(1):10460. https://doi.org/10.1038/s41467-024-54825-7

Herring T, King R, Floyd M, et al (2018) Introduction to GAMIT/GLOBK release 10.7. Tech. rep., Mass. Instit. of Technol., Cambridge

Huss M (2013) Density assumptions for converting geodetic glacier volume change to mass change. Cryosphere 7(3):877–887. https://doi.org/10.5194/tc-7-877-2013

Ishigaki M, Le Bail K, Nilsson T, et al (2026) Exploring reasons for the ITRF2020 VLBI scale drift. J Geodesy 100(36). https://doi.org/10.1007/s00190-026-02057-6

Kaufmann G, Wolf D (1996) Deglacial land emergence and lateral upper-mantle heterogeneity in the Svalbard Archipelago–II. Extended results for high-resolution load models. Geophys J Int 127(1):125–140. https://doi.org/10.1111/j.1365-246X.1996.tb01539.x

Kern L, Krasna H, Böhm J (2024) Verifying the impact of additional breaks in station coordinates on VLBI scale drift. Vienna,(Presentation EGU24-16905; EGU General Assembly 2024)

Kern L, Krásná H, Nothnagel A et al (2025) Terrestrial reference frame scale drift anomalies in VLBI and the contribution of Ny-Ålesund radio telescopes. Earth Planets Space 77(1):40. https://doi.org/10.1186/s40623-025-02159-z

Khan SA, Sasgen I, Bevis M, et al (2016) Geodetic measurements reveal similarities between post–last glacial maximum and present-day mass loss from the greenland ice sheet. Sci Adv 2(9). https://doi.org/10.1126/sciadv.1600931

Khan SA, Bamber JL, Rignot E, et al (2022) Greenland mass trends from airborne and satellite altimetry during 2011–2020. J Geophys Res: Earth Surf 127(4). https://doi.org/10.1029/2021JF006505

Kierulf HP, Pettersen B, McMillan D et al (2009) The kinematics of Ny-Ålesund from space geodetic data. J Geodynamics 48:37–46. https://doi.org/10.1016/j.jog.2009.05.002

Kierulf HP, Plag HP, Kohler J (2009) Measuring surface deformation induced by present-day ice melting in Svalbard. Geophys J Int 179(1):1–13. https://doi.org/10.1111/j.1365-246X.2009.04322.x

Kierulf HP, van Pelt WJJ, Petrov L et al (2021) Seasonal glacier and snow loading in Svalbard recovered from geodetic observations. Geophys J Int 229(1):408–425. https://doi.org/10.1093/gji/ggab482

Kierulf HP, Kohler J, Boy JP et al (2022) Time-varying uplift in Svalbard-an effect of glacial changes. Geophys J Int 231(3):1518–1534. https://doi.org/10.1093/gji/ggac264

Krasna H, Jaron F, Gruber J, et al (2021) Baseline-dependent clock offsets in VLBI data analysis. J Geodesy 95(126). https://doi.org/10.1007/s00190-021-01579-5

Lau HCP, Austermann J, Holtzman BK, et al (2021) Frequency dependent mantle viscoelasticity via the complex viscosity: cases from Antarctica. J Geophys Res: Solid Earth 126(11). https://doi.org/10.1029/2021JB022622

Le Bail K, Ishigaki M, Mouyen M et al (2023) The impact of station position modelling on terrestrial reference frames. Presentation; IUGG General Assembly, Berlin

Le Bail K, Ishigaki M, Nilsson T, et al (2026) Monitoring VLBI instrumentation for accurate terrestrial reference frames. In: International association of geodesy symposia. Springer, Berlin. https://doi.org/10.1007/1345-2026-316

Li Y, Wei E, Wei N (2024) Noise analysis of irregularly sampled vlbi position time series using maximum likelihood estimation. Adv Space Res 73(6):2892–2906. https://doi.org/10.1016/j.asr.2023.12.030

MacMillan D (2017) EOP and scale from continuous VLBI observing: CONT campaigns to future VGOS networks. J Geodesy 96(47):819–829. https://doi.org/10.1007/s00190-017-1003-4

Mankoff KD, Fettweis X, Langen PL et al (2021) Greenland ice sheet mass balance from 1840 through next week. Earth Syst Sci Data 13(10):5001–5025. https://doi.org/10.5194/essd-13-5001-2021

Mémin A, Rogister Y, Hinderer J et al (2011) Secular gravity variations at Svalbard (Norway) from ground observations and GRACE satellite data. Geophys J Int 184(3):1119–1130. https://doi.org/10.1111/j.1365-246X.2010.04922.x

Mémin A, Hinderer J, Rogister Y (2012) Separation of the geodetic consequences of past and present ice-mass change: influence of the topography with application to Svalbard (Norway). Pure Appl Geophys 169:1357–1372

Mémin A, Spada G, Boy JP et al (2014) Decadal geodetic variations in Ny-Ålesund (Svalbard): role of past and present ice-mass changes. Geophys J Int 198(1):285–297. https://doi.org/10.1093/gji/ggu134

Meza-Cala JC, Minakov A, Faleide JI et al (2024) Late cenozoic intraplate volcanism as a trigger for hydrothermal venting in the arctic southwestern Eurasia basin. Commun Earth Environ 5(1):654. https://doi.org/10.1038/s43247-024-01843-4

Mielke CA, Karegar MA, Gerdener H, et al (2025) GNSS observations of the land uplift in South Africa: implications for water mass loss. J Geophys Res: Solid Earth 130(4). https://doi.org/10.1029/2024JB030350

Minakov A (2018) Late Cenozoic lithosphere dynamics in Svalbard: Interplay of glaciation, seafloor spreading and mantle convection. J Geodyn 122:1–16. https://doi.org/10.1016/j.jog.2018.09.009

Mitrovica JX, Gomez N, Morrow E et al (2011) On the robustness of predictions of sea level fingerprints. Geophys J Int 187(2):729–742. https://doi.org/10.1111/j.1365-246X.2011.05090.x

Moholdt G, Maton J, Kohler J (2021) Frontal ablation of svalbard tidewater glaciers. https://doi.org/10.21334/NPOLAR.2021.D1D08FAC, https://doi.org/10.21334/NPOLAR.2021.D1D08FAC, [Dataset]

Morris A, Moholdt G, Gray L (2020) Spread of svalbard glacier mass loss to barents sea margins revealed by cryosat-2. J Geophys Res: Earth Surf 125(8). https://doi.org/10.1029/2019JF005357

Naganawa K, Kazama T, Fukuda Y et al (2022) Updated absolute gravity rate of change associated with glacial isostatic adjustment in Southeast Alaska and its utilization for rheological parameter estimation. Earth Planets Space 74(1):116. https://doi.org/10.1186/s40623-022-01666-7

Nield GA, Barletta VR, Bordoni A et al (2014) Rapid bedrock uplift in the Antarctic Peninsula explained by viscoelastic response to recent ice unloading. Earth Planet Sci Lett 397:32–41. https://doi.org/10.1016/j.epsl.2014.04.019

Nordli Ø, Wyszyński P, Gjelten H, et al (2020) Revisiting the extended Svalbard Airport monthly temperature series, and the compiled corresponding daily series 1898–2018. Polar Res 39(3619)

Nothnagel A, Krásná H, Urban P (2026) Impact of imminent corrections to ionospheric calibrations of legacy geodetic vlbi observations. J Geodesy (submitted)

Omang OCD, Kierulf HP (2011) Past and present-day ice mass variation on Svalbard revealed by superconducting gravimeter and GPS measurements. Geophys Res Lett 38(L22304). https://doi.org/10.1029/2011GL049266

Paxman GJG, Lau HCP, Austermann J, et al (2023) Inference of the timescale-dependent apparent viscosity structure in the upper mantle beneath greenland. AGU Adv 4(2). https://doi.org/10.1029/2022AV000751

Petrov L, Boy JP (2004) Study of the atmospheric pressure loading signal in VLBI observations. J Geophys Res 109(B03405). https://doi.org/10.1029/2003JB002500

Plag H, Pearlman M (2009) Global geodetic observing system: meeting the requirements of a global society on a changing planet in 2020. Springer, Berlin. https://doi.org/10.1007/978-3-642-02687-4

Rajner M (2018) Detection of ice mass variation using GNSS measurements at svalbard. J Geodyn 121:20–25. https://doi.org/10.1016/j.jog.2018.06.001

Rajner M (2025) Gnss sites at hornsund reveal increase of land uplift rate due to recent acceleration of deglaciation at svalbard. Reports Geodesy Geoinform 120:96–100. https://doi.org/10.2478/rgg-2025-0020

Sato T, Boy JP, Tamura Y et al (2006) Gravity tide and seasonal gravity variation at Ny-Ålesund, Svalbard in Arctic. J Geodyn 41(1):234–241. https://doi.org/10.1016/j.jog.2005.08.016

Sato T, Okuno J, Hinderer J et al (2006) A geophysical interpretation of the secular displacement and gravity rates observed at ny-Ålesund, svalbard in the arctic-effects of post-glacial rebound and present-day ice melting. Geophys J Int 165(3):729–743. https://doi.org/10.1111/j.1365-246X.2006.02992.x

Schmidt LS (2022) Cryogrid simulations of svalbard mass balance, refreezing and runoff, 1991–2022. https://doi.org/10.21343/NCWC-S086

Schmidt LS, Schuler TV, Thomas EE et al (2023) Meltwater runoff and glacier mass balance in the high arctic: 1991–20 22 simulations for svalbard. Cryosphere 17(7):2941–2963. https://doi.org/10.5194/tc-17-2941-2023

Schuler T, Kohler J, Elagina N et al (2020) Reconciling svalbard glacier mass balance. Front Earth Sci 8:156. https://doi.org/10.3389/feart.2020.00156

Schuler TV, Benestad RE, Isaksen K, et al (2025) Svalbard's 2024 record summer: an early view of arctic glacier meltdown? Proc Natl Acad Sci 122(34). https://doi.org/10.1073/pnas.2503806122

Schyberg H, Yang X, Køltzow MAØ, et al (2020) Arctic regional reanalysis on single levels from 1991 to present. https://doi.org/10.24381/cds.713858f6

Selway K, Smirnov MY, Beka T, et al (2020) Magnetotelluric constraints on the temperature, composition, partial melt content, and viscosity of the upper mantle beneath svalbard. Geochem Geophys Geosyst 21(5). https://doi.org/10.1029/2020GC008985

Smith B, Jelley BP, Dickinson S, et al (2024) Atlas/icesat-2 l3b gridded antarctic and greenland height change, version 4. https://doi.org/10.5067/ATLAS/ATL15.004, http://nsidc.org/data/atl15/versions/4

Steffen H, Kaufmann G (2005) Glacial isostatic adjustment of Scandinavia and northwestern Europe and the radial viscosity structure of the Earth's mantle. Geophys J Int 163(2):801–812. https://doi.org/10.1111/j.1365-246X.2005.02740.x

Tangen O, Kierulf HP, Himle S (2024) Local ties and repeated stability measurements in ny-Ålesund. In: Behrend D, Baver K, Armstrong K (eds) Proceedings of the 13th general meeting of the international VLBI service for geodesy and astrometry. Goddard Space Flight Center. Greenbelt, MD 20771, pp 20–24

Titov O, Krásná H (2018) Measurement of the solar acceleration using the Earth scale factor. Astronomy Astrophys 610(A36). https://doi.org/10.1051/0004-6361/201731901

Wang J, Ge M, Balidakis K, et al (2025) Integrated processing of GPS and VLBI at the observation level. J Geodesy 99(60). https://doi.org/10.1007/s00190-025-01984-0

Weerdesteijn MFM, Conrad CP (2024) Recent ice melt above a mantle plume track is accelerating the uplift of Southeast Greenland. Commun Earth Environ 5(1):791. https://doi.org/10.1038/s43247-024-01968-6

Weerdesteijn MFM, Conrad CP, Naliboff JB (2022) Solid earth uplift due to contemporary ice melt above low-viscosity regions of the upper mantle. Geophys Res Lett 49(17). https://doi.org/10.1029/2022GL099731

Westermann S, Ingeman-Nielsen T, Scheer J et al (2023) The cryogrid community model (version 1.0): a multi-physics toolbox for climate-driven simulations in the terrestrial cryosphere. Geosci Model Dev 16:2607–2647. https://doi.org/10.5194/gmd-16-2607-2023

Williams SDP, Bock Y, Fang P et al (2004) Error analysis of continuous GPS position time series. J Geophys Res 109:1–19. https://doi.org/10.1029/2003JB002741

Yi S, Hong D (2025) Survey-based the axis-offset for the sejong vlbi antenna. Sejong VLBI Technical Report 2025-01-EN https://unlimited.ethz.ch/download/attachments/352315134/Survey-Based%20the%20Axis-Offset%20for%20the%20Sejong%20VLBI_final.pdf?version=1&modificationDate=1754988628152&api=v2

Publisher's Note Springer Nature remains neutral with regard to jurisdictional claims in published maps and institutional affiliations.